Numerical Simulations of Electron Tunneling Currents in Water †

ARTICLE *in* THE JOURNAL OF PHYSICAL CHEMISTRY A · JULY 2002

Impact Factor: 2.69 · DOI: 10.1021/jp025813j · Source: arXiv

3 AUTHORS, INCLUDING:

Michael Galperin
University of California, San Diego
82 PUBLICATIONS **2,503** CITATIONS

Numerical simulations of electron tunneling in water

Alex Mosyak and Abraham Nitzan
School of Chemistry, Tel Aviv University, Tel Aviv 69978, Israel

Ronnie Kosloff
The Institute of Chemistry and the Fritz Haber Institute, The Hebrew University of Jerusalem, Israel

(Received 8 May 1995; accepted 16 August 1995)

Electron tunneling through molecular layers has long been under study in conjunction with electron tunneling microscopy. More recently solvent effects on the tunneling matrix elements associated with electron transfer problems and with ''underwater'' electron tunneling microscopy have come under discussion. This paper describes the results of computer simulations of electron tunneling through frozen water layers. A water layer ($\sim$10 Å) is confined between two electrodes, and is equilibrated and evolved in time in order to generate an ensemble of barrier configurations. The electron–(classical) water interaction is represented by a suitable pseudopotential. It is assumed that the water dynamics is negligible on the time scale of the tunneling process, so tunneling is studied for the resulting group of frozen configurations. Several numerical methods for evaluating the transmission through such disordered barriers are described and compared. It is shown that tunneling probabilities as low as 10^{-10} can be calculated with sufficient accuracy. We find that tunneling in this system cannot be described by averaging over one-dimensional paths. Furthermore, in contrast to common practice which assumes that the barrier to tunneling may be estimated by lowering the bare (vacuum) barrier by a magnitude associated with the electronic dielectric response of water taken as a dielectric continuum, the simulations show that transmission is strongly reduced due to the fact that much of the physical barrier space is blocked by the practically impenetrable oxygen cores. The tunneling probability significantly depends on the water configuration in the barrier, in particular on the orientational distribution of the water molecules. These observations suggest that external variables such as temperature and electric field will affect the tunneling through their effect on the water density and orientation, in addition to the effect of these variables on the bare (vacuum) tunneling. © *1996 American Institute of Physics.* [S0021-9606(95)50943-1]

I. INTRODUCTION

Electron tunneling in a condensed phase environment is a very long studied subject which is usually considered within simple one-dimensional modes involving well-defined potential barriers and impurity (resonance) states in such barriers. A substantial amount of study has also focused on disordered barriers[1], and in the last decade, on the effect of barrier dynamics on tunneling process. An important class of processes dominated by tunneling is electron transfer. Theoretical treatments of these processes often focus on the energetics and dynamics of the donor and acceptor levels, representing the tunneling process itself by a parameter (''electronic coupling'') in the resulting rate expressions. In the nonadiabtic limit such expressions take the form

$$k_{et} = |J|^2 F, \tag{1}$$

where J is the ''electronic coupling'' and F contains information associated with nuclear motion. In the Marcus[2] theory F is essentially the probability of the donor and acceptor levels becoming degenerate in the course of the nuclear (solvent) motion. The success of this approach indicates that in many cases the rate is determined primarily by this probability, while solvent-induced variations in the magnitude of the electronic coupling are apparently less important or at least their effect is absorbed in the parameter J. In the language of the spin–boson model, coupling to the solvent enters into the diagonal elements of the spin Hamiltonian and is often disregarded in the nondiagonal elements.[3]

Consider, however, electron transfer from a solute to a metal electrode in cases where the donor level is far above the electrode Fermi energy E_F. In this case the solvent-induced fluctuations in the position of the donor level relative to E_F are relatively unimportant (since degeneracy between donor and acceptor always exists) and the main role of the solvent may be in affecting the electronic wave functions. In such situations we expect solvent effects to manifest themselves more strongly in the nonadiabatic coupling itself.

Following Marcus[2] it has become standard to treat the solvent effect on electron transfer using a continuum dielectric picture of the solvent. This approach seems reasonable when the main solvent effect on electron transfer indeed arises from fluctuations in the donor and acceptor energy levels. These fluctuations are then described using the macroscopic solvent polarization through the frequency-dependent dielectric response. A related more rigorous approach is based on the spin–boson Hamiltonian, where the parameters of the boson Hamiltonian and of the spin–boson coupling are derived from the continuum dielectric model. No such simplification seems physically straightforward for the solvent effect on the nondiagonal electronic coupling, at least in cases where this coupling is associated with a tunneling path which goes through the liquid. Obviously, the

potential barrier and therefore the tunneling probability are strongly dependent on the instantaneous solvent structure in the space between the donor and acceptor.

The motivation for the present study comes from recent advances in electrochemical scanning tunneling microscopy which involves situations of the type described above. Figure 1 presents seven one-dimensional potential barriers for the tunneling of an electron through water, together with the corresponding tunneling probabilities. These potentials were calculated along the shortest (normal) path connecting two parallel electrodes separated by 10 Å in water, for different water configurations sampled from an equilibrium trajectory. The corresponding vacuum potential is assumed to be a symmetric square well of height $V_0=5$ eV and the displayed tunneling probabilities are calculated for the incident electron energy 3.5 eV. The water–water, water–metal, and electron–water potential used in this calculation are described in Sec II.

The large dispersion in the instantaneous potentials and in the corresponding tunneling probabilities raises a question concerning the applicability of effective continuum dielectric models in such situations. Since the tunneling probability is exponentially sensitive to the barrier structure, it is not even clear whether the observed tunneling current is associated with the average over many probable configurations or is dominated by rare fluctuations in the barrier structure.[4] In this respect we recall that realistic electrochemical systems involve not only water but other solvated ions that may wander into the space between the tip and the electrode, creating even larger fluctuations in the barrier potential. It should of course be kept in mind that in reality one should consider a three-dimensional (3D) tunneling process which, as we show below, cannot be described by the one-dimensional (1D) potential cuts displayed in Fig. 1.

The static potential surfaces shown in Fig. 1 (and their 3D analogs) are relevant to the tunneling problem only if the time scale for the tunneling process is much shorter than that associated with the solvent motion. In typical scanning tunneling microscopy (STM) configurations the tunneling time [estimated from $\int dx[1/v(x)]$ where $v(x)$ is the imaginary velocity and where the integral is over the tunneling path] is of order 10^{-16} s, so that intermolecular solvent motion may indeed be ignored, and also the effect of intramolecular solvent dynamics is expected to be small. The numerical studies described below are based on static solvent configurations.

From the numerical point of view, simulations of tunneling processes are highly demanding since the quantity evaluated is often very small and therefore highly sensitive to numerical errors. Part of our effort in the present work is focused on testing and comparing several algorithms for tunneling. We find that tunneling probabilities as low 10^{-10} can be evaluated reliably, provided that resonance trapping of the tunneling particle does not take place. In the latter situation long time transients may make the computation prohibitively costly and/or stretch it to the limit of its numerical stability.

From the physical point of view, the role of the solvent in such processes has long been appreciated but is still not well understood, as exemplified by the recent debate on this issue.[5,6] Of practical importance are questions regarding the origin of the unusually low barrier observed in ''underwater''

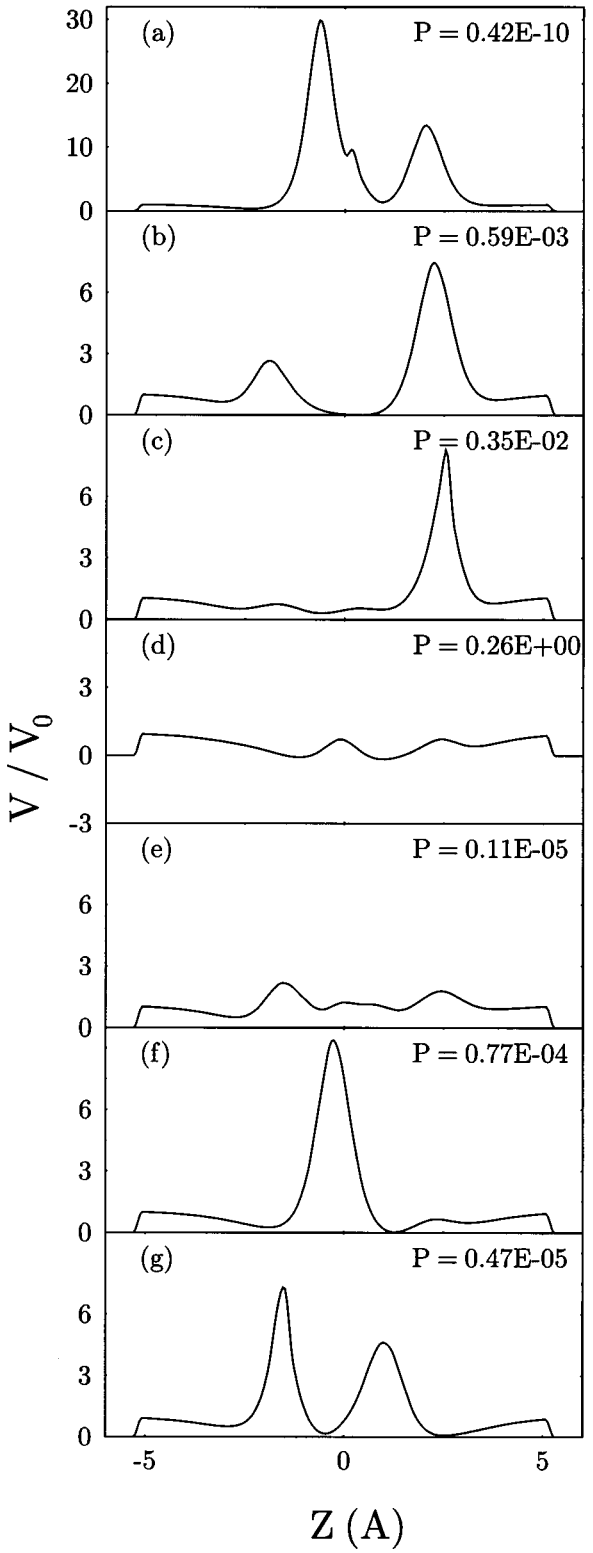

FIG. 1. One-dimensional potentials calculated along several straight paths perpendicular to and connecting the two parallel electrodes of Fig. 2(a) where the gap between the electrode contained water models is as described in the text. The electron water pseudopotential is superposed on a bare symmetric square potential of height $V_0=5$ eV that is assumed to exist between the electrodes. The displayed tunneling probabilities P are calculated for an electron with an energy of 3.5 eV.

STM experiments and the effect of solvent on the STM resolution.

A full treatment of the electron tunneling should take into account dynamic image effects associated with the electron–metal interaction[7] and the fast response associated with the solvent electronic polarizability. We[8] and others[9] have recently considered models for tunneling through a medium defined by its dielectric response, using a continuum dielectric model characterized by given boundary conditions. As expected, the effect of the fast electronic polarization is found to dominate the solvent effect on the tunneling process in this model, while the contribution of the solvent nuclear motion is relatively small. In the present work we focus on issues associated with the role played by the distribution of the instantaneous configurations of the barrier. We therefore disregard the dynamical effects of the electronic polarization of the electrode, and assume that its effect is already included in the given vacuum potential barrier. For the same reason we disregard the actual geometry of the STM experiment, and consider tunneling between two planar parallel electrodes. We also assume that the solvent nuclei are frozen on the time scale of the tunneling process. The effect of the solvent electronic polarizability is partially taken care of by representing it as an effective two-body potential. A simulation based on a similar approach with a cruder numerical algorithm was recently reported by Schmickler.[10]

The numerical codes constructed in the present work are used to examine the sensitivity of the tunneling process to the instantaneous solvent configuration, i.e., the instantaneous shapes of the barrier potential. Raikh and Ruzin[4] have suggested that such processes may be dominated by rare, favorable barrier configurations. In order to address this issue, one needs a way to generate such configurations and to compute their probability, a task that we leave for future work. Here we show that temperature and external field effects on the tunneling probability have a non-negligible contribution, resulting from the effect of these variables on the equilibrium distribution of barrier structures. We also study the effect of dimensionality on the tunneling probability and, in particular, address the validity of approximating tunneling in three dimensions by the corresponding 1D process along the shortest possible path, as is done in most theoretical models. Obviously this should not work for any given solvent configuration, but we show that this procedure is invalid also for the average (over configurations) tunneling probability.

Our physical model is described in Sec. II and a brief description of the numerical procedures is given in Sec. III. Section IV describes and discusses our numerical results and Sec. V is the conclusion.

II. THE SIMULATION MODEL

The physical system simulated in this work is a rectangular slab of water molecules (density 1 g/cm^3) confined along the z axis by two electrodes separated by 10 Å, and subjected to periodic boundary conditions in the other x and y directions. The system size in the x and y directions is taken to be 23.5 Å. This system contains 192 water molecules. In some of our computer experiments we have used a system more akin to a STM setup, where a ''tip'' protrudes into the potential barrier as seen in Fig. 2.[11] The tip is taken to be rectangular, with its xy cross section and its protruding length taken to be 3×3 Å^2 and 3.3 Å, respectively.[11] This configuration was generated from the former by artificially cutting off the barrier (both the bare barrier and the water part) in the designated tip volume. This procedure does not account for the real water structure near the tip, but may still be used for our main purpose—investigating the qualitative effect of the solvent on the transmission probability and on the spatial resolution associated with the tunneling current.

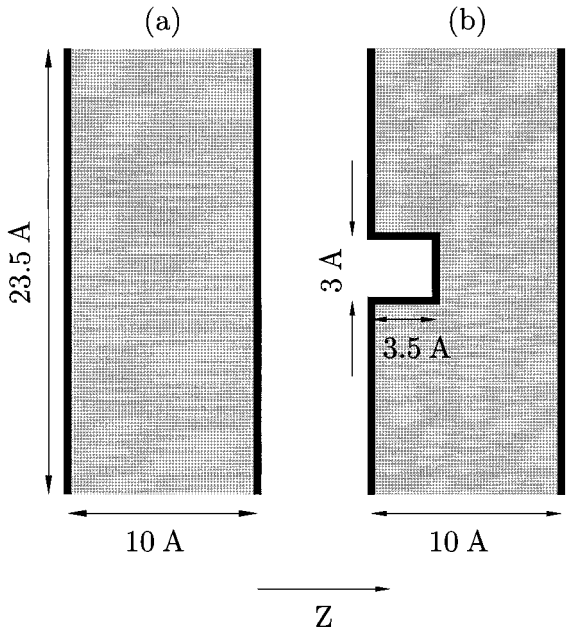

FIG. 2. A schematic two-dimensional display of the configurations used in the model calculation reported in this paper. (a) Two parallel electrodes. (b) Two parallel electrodes with an additional rectangular tip. Note that the displayed rectangular shape as well as the dimensions are defined only within the grid resolution.

The water configurations are generated by propagating the water molecules under their mutual interaction together with the confining water–wall potential. The former was taken to be a flexible RWKM-2 water–water potential as used in our earlier electron–water studies while the latter was adopted from Hautman *et al.*,[12] a 9-3 potential:

$$V_W(z)=\frac{A}{z^9}-\frac{B}{z^3} \tag{2}$$

for each H and O atom, where z is the distance from the surface, with the parameters A and B chosen to fit a spherical water–gold surface interaction. As described below, this potential was sometimes modified in order to examine the influence on the tunneling probability of changing the distribution of the water configurations.

The potential experienced by the electron arises from the walls and from the electron–water interaction as follows:

$$V = V_B + V_{eW}, \tag{3}$$

where V_B is the bare, ''vacuum'' potential associated with the walls and V_{eW} is the electron–water interaction. In the present work V_B was modeled as a symmetric square barrier of height 5 eV, i.e.,

$$V_B(x,y,z) = \begin{cases} 0 & |z| > d/2 \\ 5 \text{ eV} & |z| < d/2 \end{cases}, \tag{4}$$

where d (typically 10 Å) is the distance between electrodes. It should be clear that the numerical procedure allows any given choice for this bare barrier potential, including the possibility of an external electric field (i.e., potential gradient) and a more realistic form for the electron–electrode image potential.

For the electron–water interaction V_{eW}, we have used the pseudopotential developed by Barnett *et al.*[13] which was used in our earlier electron–water simulations. This potential contains, in addition to Coulomb exchange and exclusion contributions, terms associated with the atomic polarizability of the oxygen and hydrogen constituents, which are inversely proportional to the quartic power of the distance from the corresponding atom. In our numerical studies we have sometimes turned off this part of the electron–water interaction in order to investigate the role played by the electronic water polarizability on this level of description.

While the electron–water pseudopotential employed here has been successful in reproducing some energetic and dynamical properties of the hydrated electron, its applicability for the present problem is questionable. Once the energies of the initial and final electronic levels have been fixed, the remaining solvent effects on electron tunneling can potentially arise from the following factors: (1) The position, on the energy scale, of the ''conduction band'' of the pure solvent. By conduction band we mean extended electronic states of an *excess* electron in the neutral solvent configuration. (2) The hard cores of the atomic constituents, in the present case the water oxygens, which make a substantial part of the physical space inaccessible to the electron. (3) The possibility that rare fluctuations in the solvent structure contribute substantially to the overall tunneling probability. Factors (2) and (3) are usually disregarded in theories of electron transfer, while a common practice is to account for the first factor by setting the potential barrier height at a value, below the vacuum level, determined by the contribution of the solvent electronic polarizability. This value can be estimated as the Born energy of a point charge in a cavity of intermolecular dimensions, say a radius of a ~ 5 a.u., in a continuum with the proper dielectric constant, here the optical dielectric constant of water, $\epsilon_\infty = 1.88$. This yields $e^2(2a)^{-1}[\epsilon_\infty^{-1} - 1] \sim -1.3$ eV, the same order as the result of a more rigorous calculation by Schmickler and Henderson,[5(a)] and in agreement with the experimental results on photoemission into water.[14] This value is taken as an estimate for the position, relative to the vacuum energy, of the bottom of the conductivity band of water. It should be noted that this number was obtained for an infinite bulk of water, and should be regarded as an upper limit for the present problem. Moreover, due to the high repulsive cores of the oxygen atoms, the structure of the corresponding electronic wave functions may be a complicated function of position, implying a complex and winding path for an electron of this energy. Therefore, replacing the vacuum barrier by a similar barrier of lower height is not necessarily a good approximation.

An adequate electron–water pseudopotential should account for both the energy of the conduction band and the structure of the corresponding wave functions. However the pseudopotential employed here is not good enough in this sense: Since solvent polarizability effects were not incorporated as a many-body interaction, it is expected to underestimate the depth of the conduction band below the vacuum level. Indeed, a similar model used by Rossky and coworkers in their simulations of the solvated electron, yielding results for energetics and dynamics very similar to ours, puts the position of this band slightly *above* the vacuum level.[15]

For this reason, our simulations cannot reproduce the absolute magnitude of the tunneling probability. However if we assume, in accordance with the results of Schmickler and Henderson,[5(a)] that the magnitude of the solvent-induced barrier lowering is a constant which does not depend on the other parameters of the simulation, then this constant may be incorporated into the bare barrier height, simply shifting the energy scale of the results shown below. Obviously this procedure is not entirely satisfactory, and we leave for future work the incorporation of many-body polarizability effects into the model.[16]

III. THE NUMERICAL PROCEDURE

For each static water configuration generated as described above, we have to compute the tunneling probability for an electron in the complicated 3D potential surface (3). In the calculations described below the electron wave function was represented on a rectangular $16 \times 16 \times 1024$ lattice where the barrier occupies $16 \times 16 \times 49$ lattice sites about the origin of the z axis. The lattice spacings are 2.77 a.u. (1.47 A) in the x and y directions and 0.4 a.u. (0.21 Å) in the z direction. The tip dimensions in these lattice units are $2 \times 2 \times 16$. We have examined three numerical procedures for evaluating tunneling probabilities.

A. Propagation of an electron wave packet through the barrier

In this procedure an initial wave packet located entirely to the left (say) of the barrier and moving toward the barrier, is propagated in time until the ''collision'' with the barrier has ended, i.e., until the probability that the electron is in the barrier region has fallen below a predetermined margin. The time evolution

$$\Psi(t) = \hat{U}(t)\Psi(0) = \exp\left(-\frac{1}{\hbar}\hat{H}t\right)\Psi(0) \tag{5}$$

is executed using the Chebychev polynomial expansion of the time evolution operator.[17,18] To this end the Hamiltonian is first renormalized and shifted,

$$\hat{H}_N=\frac{\hat{H}-\hat{I}\overline{E}}{\Delta E/2}, \tag{6}$$

where $\overline{E}=(E_{\min}+E_{\max})/2$, $\Delta E=E_{\max}-E_{\min}$, and $E_{\min}$ and $E_{\max}$ are, respectively, the lower and upper limits on the spectrum of the grid Hamiltonian. Such bounds are easily determined since the grid restricts the highest possible representable momentum in any direction i to $P_i^{\max}=\pi\hbar/\Delta r_i$ where Δr_i is the corresponding grid spacing. Thus

$$E_{\min}=V_{\min}, \quad E_{\max}=V_{\max}+\sum_i (P_i^{\max})^2/2m. \tag{7}$$

The scaling (6) has the effect that the spectrum of the normalized Hamiltonian lies in the range $(-1,1)$. The time evolution operator then takes the form

$$\begin{aligned}\Psi(\mathbf{r},t)&=e^{-i\overline{E}t/\hbar}e^{-i[\Delta Et/2\hbar]\hat{H}_N}\Psi(\mathbf{r},0)\\&=e^{-i\overline{E}t/\hbar}\sum_{n=0}^{N} a_n\left(\frac{\Delta Et}{2\hbar}\right)\Phi_n(\mathbf{r}),\end{aligned} \tag{8}$$

where $a_n(x)$ are essentially the Bessel functions $J_n(x)$,

$$a_n(x)=(2-\delta_{n0})J_n(x) \tag{9}$$

and where Φ_n denotes the functions obtained by operating with the complex Chebychev polynomials of the order n of $\hat{H}_N$ on the initial function $\Psi(0)=\Psi(\mathbf{r},t=0)$. These can be computed recursively:

$$\begin{aligned}&\Phi_0=\Psi(0), \quad \Phi_1=-i\hat{H}_N\Psi(0),\\ &\text{and}\\ &\Phi_{n+1}=-2i\hat{H}_N\Phi_N+\Phi_{n-1}.\end{aligned} \tag{10}$$

The repeated operations of the Hamiltonian in Eq. (10) are executed using the fast Fourier transform algorithm.[18] In practical application the sum in Eq. (8) can be truncated at a finite value of terms N, which satisfies $N>\Delta Et/2\hbar$.

The initial wave packet is chosen to be of the form

$$\Psi(\mathbf{r},0)=Ae^{ik_{0x}x}e^{ik_{0y}y}g(z), \tag{11}$$

where k_x and k_y are the components of the initial wave vector in the directions parallel to the barrier, $g(z)$ is a wave packet in z, centered to the left of the barrier, and where A is a normalization constant. It is important for the following analysis that $g(z)$ will contain only wave vectors in the positive z direction, so that there is a one to one correspondence between k_z and the energy E (for the given k_x and k_y). The final time t_f is determined such that $\int_{\text{barrier}}|\Psi(\mathbf{r},t)|^2d\mathbf{r}$ is smaller than a predetermined small number, say 10^{-8}. The transition probability from an initial free particle state $\mathbf{k}_0$ to a final state $\mathbf{k}_f$ is then obtained from

$$P_{k_0\to k_f}=\frac{|\int d\mathbf{r}e^{-i\mathbf{k}_0\cdot\mathbf{r}}\Psi(\mathbf{r},0)|^2}{|\int d\mathbf{r}e^{-i\mathbf{k}_f\cdot\mathbf{r}}\Psi(\mathbf{r},t_f)|^2}. \tag{12}$$

Since the process is elastic, this will vanish unless $|\mathbf{k}_0|=|\mathbf{k}_f|$. The total transmission probability is obtained by summing Eq. (12) over all $\mathbf{k}_f$ which satisfy this condition together with $k_{fz}>0$.

B. Direct evaluation of S-matrix elements using the Møller operator propagation technique (Ref. 19)

This approach yields selected elements of the S matrix, from which transmission probabilities can be obtained $P_{\mathbf{k}_0\to\mathbf{k}_f}=|S_{\mathbf{k}_0\to\mathbf{k}_f}|^2$. The corresponding S-matrix element is calculated using the following three-step procedure outlined as follows: (1) Choose an initial wave packet $\phi_i(\mathbf{r})$ of the form $\phi_i(\mathbf{r})=A_ie^{ik_{ix}x}e^{ik_{iy}y}g_i(z)$ *centered in the barrier region*. (2) Use the Møller operator Ω_+

$$\Omega_{\pm}=\lim_{t\to\mp\infty} e^{iHt/\hbar}e^{-iH_0t/\hbar} \tag{13}$$

to obtain a wave packet of incoming waves $\phi_i^+(\mathbf{r})$,

$$\phi_i^+(\mathbf{r})=\Omega_+\phi_i(\mathbf{r}). \tag{14}$$

Operation (14) is conducted by carrying out the free evolution analytically up to time at which the wave packet is well to the left of the barrier, then using the Chebyshev algorithm (8)–(10) to bring back the packet to the interaction region under the full Hamiltonian H. (3) Use a similar procedure to construct a packet of outgoing waves by starting from the wave packet $\phi_f(\mathbf{r})=A_fe^{ik_{fx}x}e^{ik_{fy}y}g_f(z)$ and operating with Ω_-. The element $S_{\mathbf{k}_i\to\mathbf{k}_f}$ of the S matrix, with $\mathbf{k}_i=(k_{ix},k_{iy},k)$ and $\mathbf{k}_f=(k_{fx},k_{fy},k')$, where $\hbar^2k_i^2/2m=\hbar^2k_f^2/2m=E$, can now be calculated from

$$\begin{aligned}S_{\mathbf{k}_i\to\mathbf{k}_f}&=(2\pi\hbar)^{-1}\delta[E(k)-E(k')]c_f^*(k')c_i(k)\\&\times\int_{-\infty}^{\infty}dte^{iEt/\hbar}\langle\phi_f^-|e^{-i\hat{H}t/\hbar}|\phi_i^+\rangle,\end{aligned} \tag{15}$$

where

$$c(k)=\left[B(k)\frac{L_zm}{2\pi\hbar^2k}\right]^{-1} \tag{16}$$

and where $B(k)$ are the coefficients of expansion of the wave packet $g(z)$ in plane waves[20]

$$B(k)=\frac{1}{\sqrt{L_z}}\int_{-L_z/2}^{L_z/2}dze^{-ikz}g(z). \tag{17}$$

The efficiency of the present scheme results from the fact that the integral in Eq. (15) can be expressed as a rapidly converging sum over matrix elements of Chebychev polynomials of the Hamiltonian. To this end the time evolution operation in Eq. (15) is expressed as given by Eqs. (8) and (9), and the Fourier transforms of the Bessel functions are expressed by

$$\int_{-\infty}^{\infty}e^{-i\omega t}J_n(t)dt=\frac{2(-i)^n}{\sqrt{1-\omega^2}}T_n(\omega), \tag{18}$$

where T_l are the (real) Chebychev polynomials of the order l. Furthermore, using the following properties of the real and complex Chebychev polynomials

$$\begin{aligned}&T_l(-\alpha)=(-1)^lT_l(\alpha),\\&\chi_l(-i\alpha)=(-i)^lT_l(\alpha),\end{aligned} \tag{19}$$

finally leads to

$$\int_{-\infty}^{\infty} dt e^{iEt/\hbar}\langle\phi_f^-|e^{i\hat{H}t/\hbar}|\phi_i^+\rangle = \frac{4}{\Delta E\sqrt{1-\xi^2}}\left\{\langle\phi_f^-|\phi_i^+\rangle + 2\sum_{n=1}^{N}(-1)^n T_n(\xi)\langle\phi_f^-|T_n(\hat{H}_N)|\phi_i^+\rangle\right\}, \tag{20}$$

where

$$\xi = 2(\bar{E}-E)/\Delta E. \tag{21}$$

This scheme is relatively fast and accurate, and is useful for problems in which only selected final directions of the outgoing state are of interest.

C. Direct evaluation of transition probabilities using absorbing boundary conditions (ABC) Green's functions (Ref. 21)

In this procedure the Green's function

$$\hat{G}(E;\epsilon) = \frac{1}{E-\hat{H}+i\hat{\epsilon}(\mathbf{r})} \tag{22}$$

is evaluated on an appropriate grid, where $\epsilon(\mathbf{r})$ is chosen to be different from zero near the grid boundaries, far enough from the interaction region (here the tunneling barrier), and gradually diminishing to zero as the interaction region is approached from the outside. This way of imposing outgoing wave boundary conditions has proven very useful in several recent applications.[21,22] In the present application periodic boundary conditions are maintained in the x and y directions, and $\epsilon(z)$ is taken to be of the form

$$\epsilon(z) = \begin{cases} \epsilon_0\left[\dfrac{|z|-(z_{\max}-\Delta z)}{\Delta z}\right]^v, & z_{\max}\geqslant|z|\geqslant z_{\max}-\Delta z, \\ 0, & z_{\max}-\Delta z>|z|, \end{cases} \tag{23}$$

where ϵ_0, Δz, and v are suitably chosen parameters and where $z_{\max}$ is half the system size in the z direction (i.e., 108.5 Å). In the present application the values $\epsilon_0=13.6$ eV, $\Delta z = z_{\max}-5$ Å, and $v=8$ were found to give satisfactory results.[23] Once $G(E;\epsilon)$ has been evaluated, the cumulative microcanonical transition probability defined by $N(E)\equiv\Sigma_i\Sigma_f|S_{if}(E)|^2$ can be calculated from the expression[24]

$$N(E) = \tfrac{1}{2}(2\pi\hbar)^2\ \mathrm{tr}[\hat{F}\delta(E-\hat{H})\hat{F}\delta(E-\hat{H})]. \tag{24}$$

$\hat{F}$ is the flux operator, given in our case by

$$\hat{F} = \frac{i}{\hbar}[H, h(z-z_0)], \tag{25}$$

where $h(z)$ is the step function, $h(z<0)=0$; $h(z\geqslant 0)=1$, and where z_0 can be taken anywhere in the region $|z|<|z_{\max}|-\Delta z$. By expressing the δ operators in Eq. (24) in terms of the Green's functions it is found that[21]

$$N(E)\equiv\sum_i\sum_f|S_{if}(E)|^2 = 4\,\mathrm{tr}[(1-h)\epsilon G h\epsilon G^*]. \tag{26}$$

Thus $N(E)$ can be evaluated by performing a simple trace on the grid. Moreover, exact outgoing and incoming wave functions Ψ_i^+ and Ψ_f^- which correspond to the initial and final states (eigenfunctions of H_0 with energy E) ϕ_i and ϕ_f, respectively, can be computed from

$$\Psi_i^+ = \frac{1}{E-H+i\epsilon}i\epsilon\phi_i, \qquad \Psi_f^- = \frac{1}{E-H-i\epsilon}(-i\epsilon)\phi_f, \tag{27}$$

and provide a route, alternative to method B above, for evaluating state selected transition probabilities, $S_{if}=\langle\Psi_f^-|\Psi_i^+\rangle$. Finally, the transition probability from an initial incoming state ϕ_i to all possible final states can be computed[25] from the flux

$$P_i(E)\equiv\sum_f|S_{f,i}(E)|^2 = \langle\Psi_i^+|\hat{F}|\Psi_i^+\rangle. \tag{28}$$

Obviously, the applicability of the above expressions depend on our ability to evaluate the grid Green's function in an efficient and accurate way. One way to do this is by using time propagation and Fourier transformation from time to energy space as described by Kosloff.[26] The ABC Green's function is written as

$$G(E) = \frac{1}{i}\int_0^\infty dt e^{i(E+i\hat{\epsilon}-\hat{H})t} = \frac{1}{i}\sum_{n=0}^{\infty}[e^{iE\Delta t}e^{-i(\hat{H}-i\hat{\epsilon})\Delta t}]^n\int_0^{\Delta t}dt e^{iEt}e^{-i(\hat{H}-i\hat{\epsilon})t} \tag{29}$$

and the time evolution operators are represented by a suitable polynomial expansion after renormalizing the Hamiltonian as in Eq. (6). Because the presence of the absorbing potential makes these operators non-Hermitian the Chebychev expansion is unstable. Instead, an expansion in terms of Newton polynomials is used:

$$e^{-i(\hat{H}-i\hat{\epsilon})t} = \sum_{k=0}^{K}a_k(t)R_k(\hat{H}-i\hat{\epsilon}), \tag{30a}$$

where

$$R_k(z) = \begin{cases} 1, & k=0 \\ \displaystyle\prod_{j=0}^{k-1}(z-z_j), & k>0 \end{cases} \tag{30b}$$

and where z_j are a set of suitably chosen points in the complex plane. The coefficients $a_k(t)$ depend explicitly on the set $\{z\}$: Denoting $f_k(t)=\exp[-i(z_k-i\epsilon)t]$, they are obtained from the recursion relations

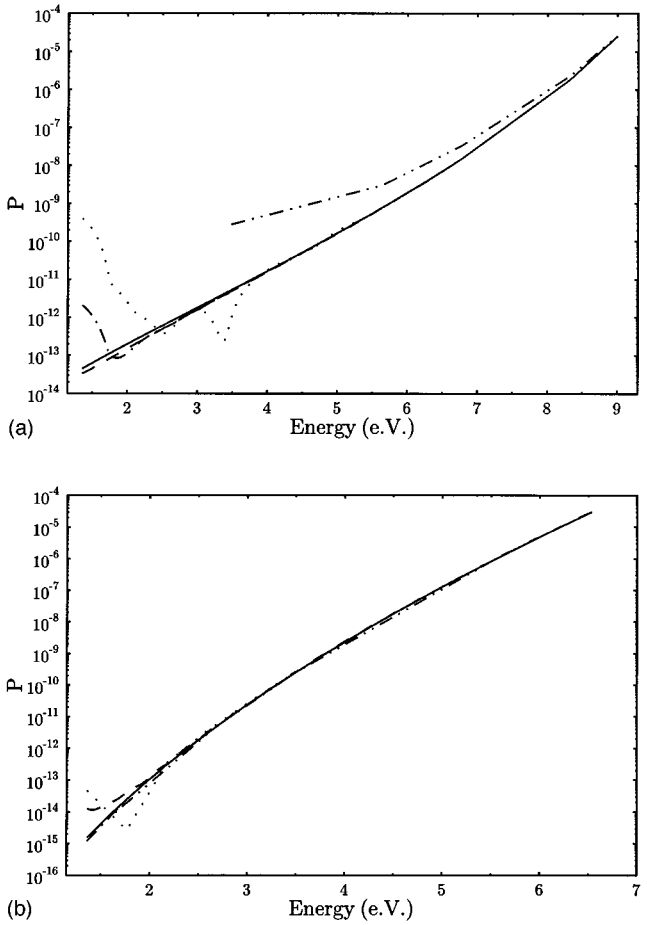

FIG. 3. (a) Tunneling probability P vs electron energy calculated for a one-dimensional rectangular barrier of width 10 Å and height 10 eV. (b) The same for an Eckart barrier, $V=V_0\,\mathrm{sech}^2(z/a)$ with $V_0=10$ eV and $a=5.26$ Å. —: analytical results; ···: direct propagation (method A); –·–: Møller operator method (method B); –···–: Green's function (method C) via Newton's expansion; – – –: Green's function by direct inversion. All calculations were done using a grid of 1024 points with spacing of 0.4 a.u. (0.21 Å). Details of the absorbing potential used in the Green's function calculations are described in the text.

$$a_k(t)=\left(f_k(t)-a_0-\sum_{j=1}^{k-1}a_j(t)\prod_{i=0}^{j-1}(z_k-z_i)\right)\Bigg/\left(\prod_{j=0}^{k-1}(z_k-z_j)\right) \tag{31}$$

with $a_0(t)=f_0(t)$ and $a_1(t)=[f_1(t)-f_0(t)]/(z_1-z_0)$. Convergence of this procedure is sensitive to the order in which contributions from different points in the set $\{z\}$ are summed. More details concerning the choice of these points and summation order are given in Ref. 26. Denoting $b_k(E,\Delta t)=\int_0^{\Delta t}e^{iEt}a_k(t)dt$ and $c_k(E,\Delta t)=e^{iE\Delta t}a_k(\Delta t)$, the Green's operator is now given by

$$G(E)=\frac{1}{i}\sum_{n=0}^{\infty}\left[\sum_{k=0}^{K}c_k(E,\Delta t)R_k(\hat{H}-i\hat{\epsilon})\right]^n \times\sum_{n=0}^{\infty}b_k(\Delta E,t)R_k(\hat{H}-i\hat{\epsilon}). \tag{32}$$

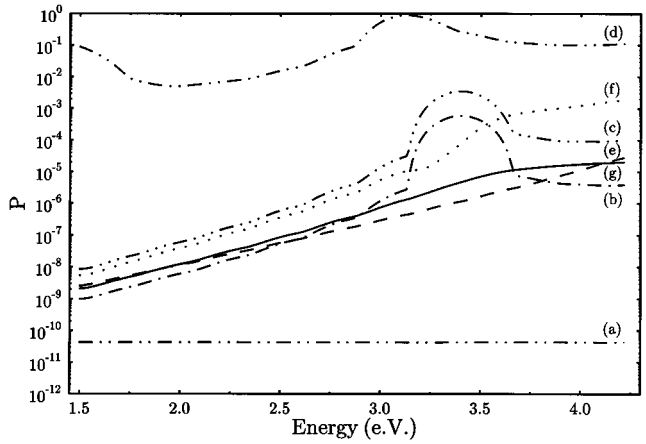

FIG. 4. Tunneling probabilities vs electron energy for the seven 1D potentials shown in Fig. 1. Different line types are used to aid the eye: (a) and (d) (–···–), (b) (–·–), (c) (–···–), (e) – – –), (f) (···), and (g) (—).

As in the Chebychev expansion, the upper bound K of the k summation has to be larger than $\Delta t\Delta E$. Also, the summation over N is truncated when the modulus of the vectors being summed becomes smaller than some predetermined small number.

Some of the results shown below were obtained using this algorithm and Eqs. (27) and (28). We have found however that this approach as well as all other methods described above suffer from a drawback common to all time evolution methods: If long time trapping of the wave packet in the barrier takes place (due to resonances) convergence can become very slow. This problem can possibly be circumvented using a modification[27] of a method proposed by Neuhauser.[28] In the present application we have found that resonance trapping constitutes a problem only for the one-dimensional calculations (see below). In these cases the grid Green's function can be evaluated by direct inversion of the grid matrix $[\mathbf{E}-\mathbf{H}+\mathbf{i}\boldsymbol{\epsilon}(\mathbf{r})]$. Some of the results shown below are based on this procedure together with Eqs. (27) and (28).

IV. RESULTS AND DISCUSSION

Comparison between the different numerical methods outlined above is made in Fig. 3. Figure 3(a) shows the tunneling probability for an electron going through a one-dimensional symmetrical rectangular barrier of a height of 10 eV and a width of 10 Å as a function of the electron energy. Shown are the exact result and the results based on the three algorithms described above. Figure 3(b) shows similar results for an Eckart barrier, $V(z)=V_0\,\mathrm{sech}^2(z/a)$, with height $V_0=10$ eV and width $a=5.29$ Å. A grid of 1024 points with a spacing of 0.4 a.u. (0.21 Å) was used in all cases. For the Green's function calculations the absorbing potential described below [Eq. (23)] was used.

It is seen that in most cases all the methods are reliable down to transition probabilities smaller than 10^{-10}, except for Newton's expansion method which does not perform as well for the square barrier. It should be emphasized that the performance of the ABC Green's function method depends

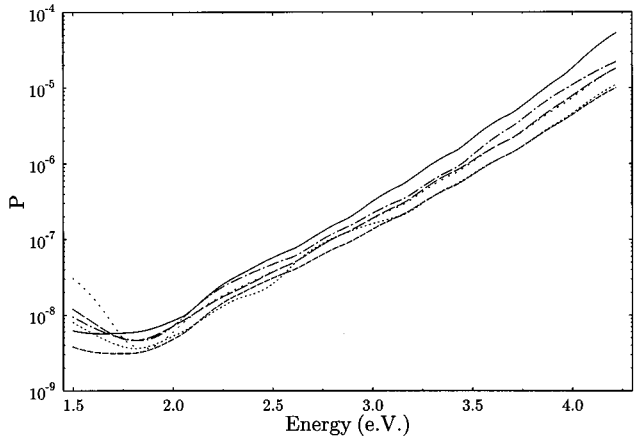

FIG. 5. Tunneling probabilities vs electron energy obtained for six water configuration samples as described in the text.

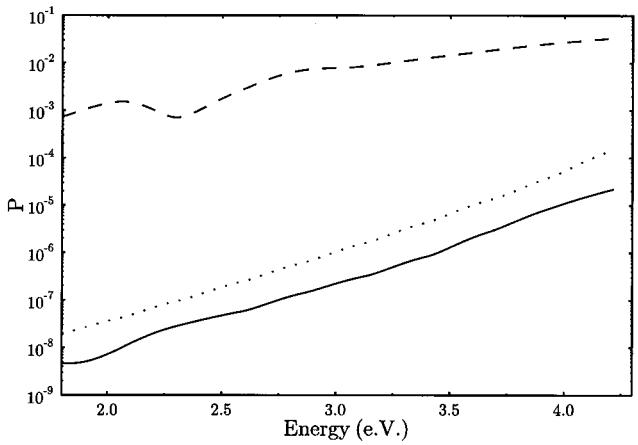

FIG. 6. Full line: Tunneling probability vs electron energy calculated for a particular three-dimensional water configuration in the barrier. (This is one of the lines shown in Fig. 5.) Dashed line: Average over 256 (per configuration) tunneling probabilities calculated for one-dimensional sections through the same configuration (see the text). Dotted line: tunneling probability through the bare rectangular barrier of height 5 eV.

on the need to compromise between smoothness of the absorbing potential and the efficiency of the absorption. The magnitude and shape of this potential have to be chosen carefully, otherwise it may bias the results when the probabilities calculated are very low. The time-dependent methods A and B perform very well in the present examples, except for the unphysical rise in the computed probabilities at very low electron energies. As discussed above these methods may perform poorly when resonance trapping takes place in the barrier.

Turning now to tunneling through simulated water layers, we show a series of results demonstrating the dependence of the tunneling process on the structure of the water layer between the electrodes. In the numerical experiments the distance between the electrodes is 10 Å, and the bare (vacuum) barrier height is 5 eV. Figure 4 shows again the tunneling probabilities associated with the seven one-dimensional potentials displayed in Fig. 1, computed by direct inversion of the matrix $[\mathbf{E}-\mathbf{H}+\mathbf{i}\epsilon(\mathbf{r})]$ and using the resulting Green's matrix in Eqs. (27) and (28). Here the tunneling probabilities are shown as functions of the incident electron energy. An important source of variation between the different results is the occurrence of resonance structures supported by some of the 1D potentials. When this happens the tunneling probability peaks considerably. However, the highest tunneling probability at all displayed energies is associated with the potential (d) in Fig. 1. The corresponding one-dimensional path appears to have missed close encounters with oxygen cores, while going near hydrogen nuclei, therefore becoming even negative at some points. The resulting barrier is very low, and the corresponding tunneling probability (Fig. 3) is extremely high relative to most other one-dimensional paths.

No such resonance structures were found among the limited set of configurations sampled in the three-dimensional case. This is seen in Fig. 5 which shows the integrated (over all final directions) transmission probabilities calculated for six configurations, obtained, at 0.4 ps apart, along a classical trajectory of the neat water at 300 K between the electrodes. The incident electron is perpendicular to the barrier and the transmission is shown as a function of the incident energy. The transition probability is seen to decrease exponentially with electron energy (the rise at low energies is probably unphysical, similar to the unphysical rise observed for low energies in Fig. 3). The variations between the results obtained for the different configurations span about half an order of magnitude and no resonance structures are seen. It should be emphasized that the one-dimensional potentials shown in Fig. 1 and used to obtain the results of Fig. 4 are all obtained from different cuts in the normal directions through these configurations. The qualitative difference observed between the three-dimensional results and the one-dimensional tunneling through the same water configurations shows that the tunneling process cannot be approximated by taking the average of one-dimensional tunneling probabilities calculated along perpendicular tunneling paths. Indeed, an attempt to do so leads to a substantial *overestimate* of the tunneling probability in this system. This is seen in Fig. 6 where the result for one of the configurations shown in Fig. 5 is displayed together with the corresponding bare barrier result and with the average over 256 (the size of our xy grid) linear tunneling paths perpendicular to the electrodes calculated from the same three-dimensional water configuration. The latter calculation is seen to overestimate the tunneling probability by several orders of magnitude. The reason for this enormous overestimate is that among the 1D linear paths there are a few that effectively go through ''holes'' in the potential barrier, as discussed above. Along these paths the potential is relatively low [as in Fig. 1(d)], and the resulting high tunneling probabilities dominate the average of one-dimensional results. These holes in the potential barrier are quite narrow, of the order of interatomic distances, and they do not contribute considerably to the three-dimensional tunneling: In order that the electron passes through such a hole it has to become rather localized in the xy plane and the

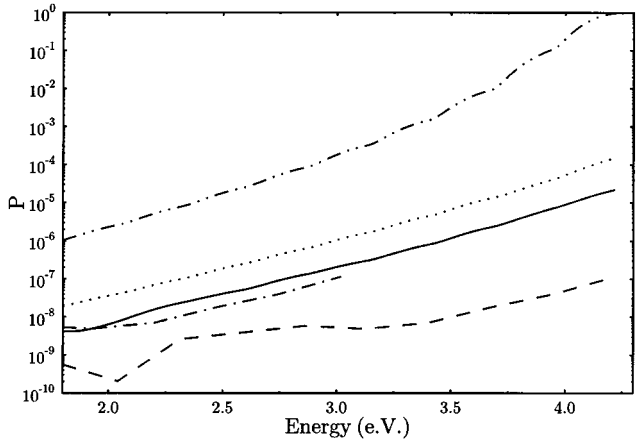

FIG. 7. Full and dotted lines are the same as in Fig. 6. Dashed line: Tunneling probability through a potential obtained by removing the attractive "polarizability" (r^{-4}) terms from the electron–water pseudopotential. Dash-dotted line: The tunneling probability obtained by superposing the electron–water interaction without the polarizability terms on rectangular barrier of height 3.8 eV. Dashed-double-dotted line: tunneling probability through a rectangular barrier of height 3.8 eV.

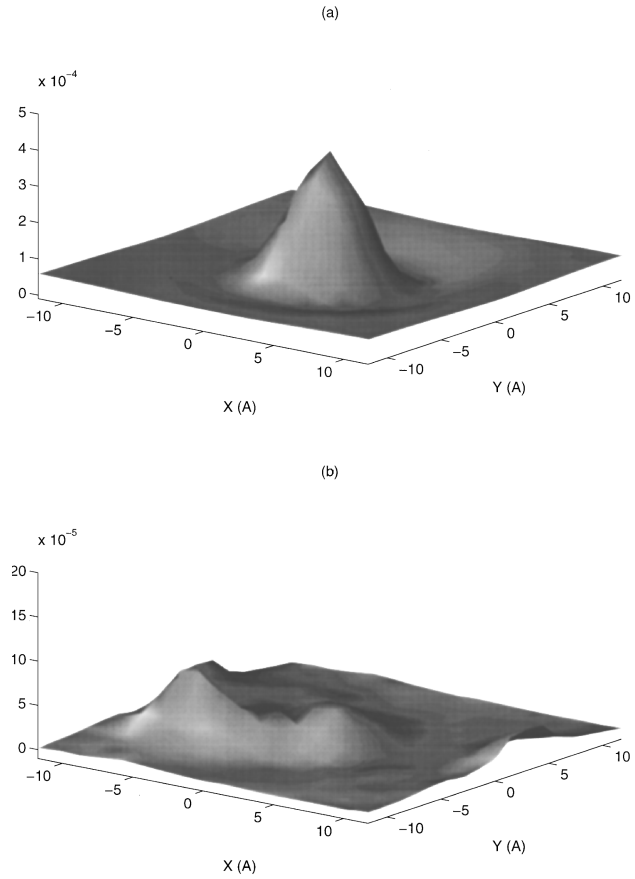

FIG. 8. The distribution of tunneling current obtained from the tip configuration [Fig. 2(b)] in the plane of the counterelectrode; (a) without water and (b) with water in the space between the electrode.

necessary localization energy will make such a path energetically unfavorable.

The electron transmission probability averaged over the configurations used in Fig. 5 is shown again in Fig. 7. Again, the incident direction is perpendicular to the barrier and the tunneling probability was integrated over all final directions. Shown are the results obtained using the full electron–water pseudopotential, as well as results of a model which does not include the polarizability, r^{-4}, terms in the pseudopotential. In addition Fig. 7 shows the transmission probability through the bare barrier (vacuum situation) as well as the result obtained by assuming a uniform lowering of the bare barrier potential by 1.2 eV, the order of the barrier lowering calculated by Schmickler and Henderson. First note that the tunneling probability calculated with our electron–water pseudopotential is lower by $\sim$ half an order of magnitude than that calculated for the bare barrier. This observation is related to the disordered nature of the barrier in the presence of water molecules and to the fact that much of the physical barrier space is now taken by essentially impenetrable oxygen cores. As discussed in Sec. I, our pseudopotential is not expected to yield a reliable estimate of the effective barrier lowering associated with the water electronic polarizability. We may attempt to account for this shortcoming by using the same pseudopotential without the r^{-4} terms, with the "dressed" barrier shifted downward by the estimated 1.2 eV. This is equivalent to shifting the horizontal (incident) energy scale of the dashed line in Fig. 7 by the same value. In turn the resulting probability (dash-dotted line in Fig. 7) should be compared with the estimate based on the continuum dielectric model, i.e, a square barrier with height uniformly reduced by 1.2 eV (the upper line in Fig. 7). Obviously the simulation results remain lower than the results of the continuum model by $\sim$2–3 orders of magnitude. Interestingly, the result obtained from the superposition of a 5 eV rectangular barrier plus the full electron–water pseudopotential (the full line in Fig. 7) and that obtained from the superposition of a 3.8 eV rectangular barrier with an electron–water pseudopotential that does not contain the polarizability term (the dash-dotted line in Fig. 7) are very close to each other. These observations suggest that the continuum dielectric model, which disregards the randomly positioned and strongly repulsive oxygen centers, strongly overestimate the tunneling probability for this system.

The effect of the water on the spatial resolution of the tunneling current in the tip configuration of Fig. 2(b) is displayed in Fig. 8. Here we show the distribution of the current density in the plane of the counterelectrode. Figure 8(a) shows the current density in this plane in the absence of water while Fig. 8(b) shows the distribution obtained in the presence of water (using a single water configuration). It is seen that the scattering of the tunneling electron by the water molecules causes a considerable loss of spatial resolution. In fact the peak of the distribution can shift its position [as seen in Fig. 9(b)] as the electron chooses a favorable tunneling path.

Coming back to the tunneling probabilities calculated for different 3D water configurations (Fig. 5), the variations seen between different configurations may look surprisingly small, however we should bear in mind that the water distri-

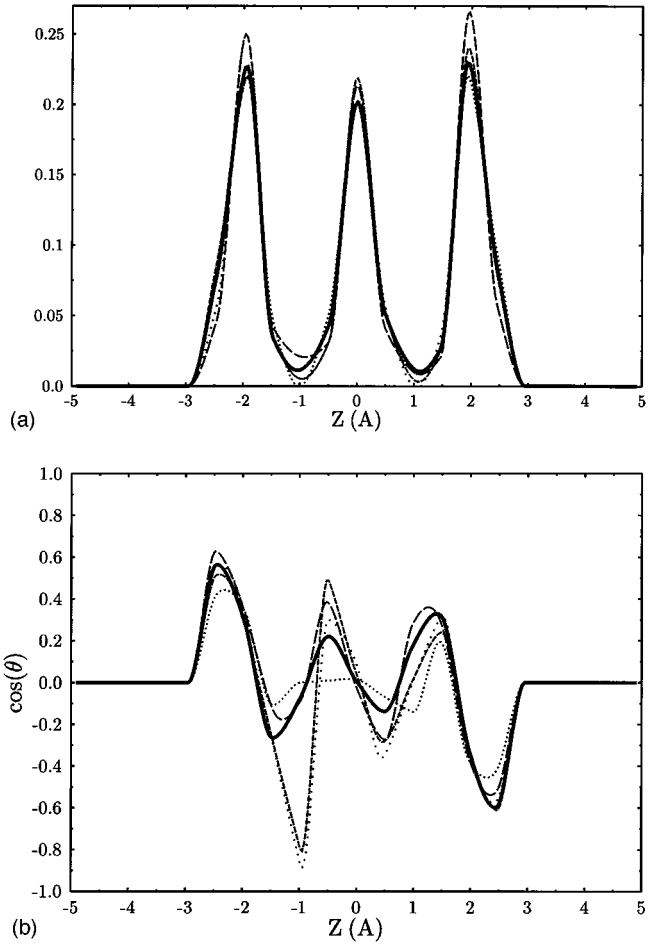

FIG. 9. (a) Water density as a function of position between the electrode. Thick line: average over 200 configurations. Four other lines: results for specific configurations randomly chosen from the same ensemble. (b) Same as for (a), for the distribution of angle θ between the water dipole and the z axis (tunneling direction).

bution in the narrow slab between the electrodes is held quite tightly by the combination of water–electrode and water–water interactions. This is seen in Fig. 9 which displays the density of water molecules (the molecular position is taken as the center of the O atoms) as function of position along the z axis. Shown in Fig. 9(a) is the average over 200 configurations sampled from a 10 ps trajectory (300 K) together with the results of four configurations randomly selected from this set. Figure 9(b) shows similar results for the distribution of water–dipole directions, represented by $\cos\theta$ where θ is the angle between the dipole and the normal to the electrode surface.

The sensitivity of the electron tunneling probability to the structure of the water layer is demonstrated in Figs. 10 and 11. In Fig. 10 we compare the tunneling probability (as a function of incident energy) for three water configurations which differ from each other by the amount of orientational ordering induced by an external electric field perpendicular to the electrodes. Note that this field is just a numerical device used to affect the molecular orientational distribution in the barrier, and the tunneling probability is calculated for the

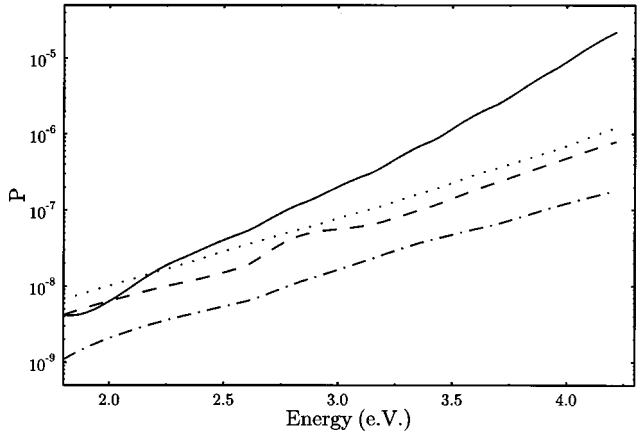

FIG. 10. Tunneling probability vs electron energy obtained for four water configurations selected from equilibrium trajectories in which the water configuration was biased by an external electrostatic field in the direction perpendicular to the electrodes. Note that the field is just a device used to affect the water configuration and it does not directly influence the electron. Full line: zero field. Dotted line: 1.7×10^8 V/cm; dashed line: 2.3×10^8 V/cm; dashed dotted line: 3.3×10^8 V/cm.

resulting frozen water configuration in the absence of the field. Also note that the field tends to order the water molecules so that their dipoles become parallel to it, opposing the structure induced by the water–wall interaction, in particular the oxygen–wall attraction, which tries to order the molecules with mirror symmetry relative to the $z=0$ plane [see Fig. 9(b)]. Another numerical way to counter the ordering induced by the latter interaction is to eliminate it altogether, using water configurations obtained from trajectories with purely repulsive interaction between the water and the wall. The effect of this structural change is shown in Fig. 11.

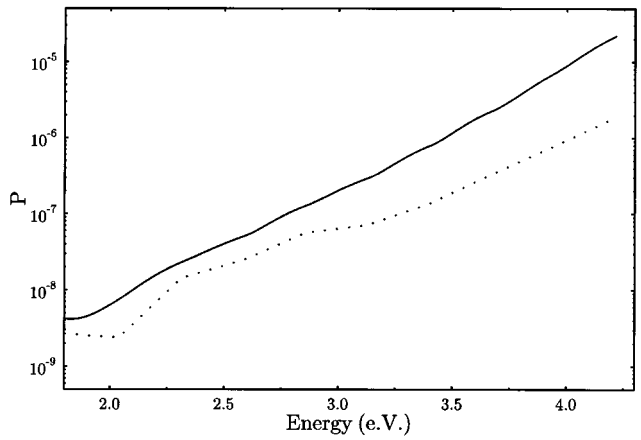

FIG. 11. Tunneling probability vs electron energy for two water configurations selected from different equilibrium ensembles associated with different magnitude of orientational ordering. Full line: A configuration obtained at 300 K in the presence of the full water–wall potential described in the text. Dotted line: A configuration calculated using a water–wall potential that does not contain the attractive interaction between the water oxygen and the wall and is therefore not restricted to a specific orientational ordering near the wall.

Both Figs. 10 and 11 show that disrupting the ordering induced by the water–wall interaction reduces the transmission probability in the system studied.

V. CONCLUSIONS

In this work we have carried out simulations of electron tunneling through thin water layers confined between two walls in order to study the effect of the barrier structure on electron tunneling. We have examined several numerical methods for evaluating tunneling probabilities and compared their performance. The model used for the electron–water pseudopotential is incomplete, in that it does not take into account the many-body nature of the water electronic polarizability. For this reason the effective barrier lowering caused by this polarizability had to be put in phenomenologically. We were able, however, to examine the effect of other Coulombic and short-range interactions on the transmission probability through such barriers. Our main conclusions are as follows.

(1) The barrier lowering caused by the electronic polarizability of the water is largely offset by the reduction in tunneling caused by the multiple scattering of the electron by the hard oxygen cores in the barrier. The result of these two opposing effects is that the overall tunneling probability through water is not significantly higher than through vacuum. (This should not be confused with saying that the workfunction for emission into water is not lowered by the effective reduction in barrier height.) It should be kept in mind though that these results were obtained in a model which disregards the many-body nature of the induced dipolar interactions.
(2) The effect of multiple scattering by the oxygen cores is to distort and diffuse the tunneling current, resulting in loss of resolution of an underwater STM signal if the tip–surface distance is large enough to accommodate water molecules.
(3) The process studied is inherently three dimensional, and attempting to describe it as a simple average over one-dimensional tunneling events leads to errors of several orders of magnitude.
(4) One-dimensional tunneling through the disordered media considered in this work were shown to be dominated by relatively rare structures with very high tunneling probabilities. We do not have any indication that this phenomenon also occurs in three dimensions, although, because of the limited sampling that could be done with our computational resources, we cannot rule out this possibility.

Our future work will focus on introducing water electronic polarizability as an integral part of the model, in order to avoid the need to account for the effect of this interaction phenomenologically.

ACKNOWLEDGMENTS

This research was supported by the US–Israel Binational Science Foundation. We thank Professor M. Urbakh and Professor D. Tannor for many helpful discussions. A.N. thanks the Alexander von Humboldt Stiftung for supporting his stay in Germany under the Humboldt Research Award Program during the time this paper was completed, and Professor W. Dieterich (University of Konstanz) and Professor G. H. F. Diercksen (MPI f. Astrophysik, Garching) for their hospitality.

[1] I. M. Lifshitz, S. A. Gredeskul, and A. Pastur, *Introduction to the Theory of Disordered Systems* (Wiley, New York, 1988), Chap. 7.
[2] R. A. Marcus, J. Chem. Phys. **24**, 966 (1956); **26**, 867, 872 (1957).
[3] Several "non-Condon" treatments of electronic transition have been published. In these treatments the dependence of the electronic coupling on intramolecular and/or solvent nuclear degrees of freedom was taken into account in various levels of approximation. For a recent treatment in the context of electron transfer theory see A. M. Kuznetsov and M. D. Vigdorovich, Chem. Phys. **176**, 539 (1993).
[4] M. E. Raikh and I. M. Ruzin, Sov. Phys. JETP **65**, 1273 (1987).
[5] (a) W. Schmickler and D. Henderson, J. Electroanal. Chem. **290**, 283 (1990); (b) W. Schmickler, *ibid*. **296**, 283 (1990).
[6] K. K. Sass and J. K. Gimzewski, J. Electroanal. Chem. **308**, 333 (1991).
[7] (a) See, for example, P. A. Serena, J. M. Soler, and N. Garcia, Phys. Rev. B **34**, 6767 (1986); (b) A. Liebsch, Phys. Scripta **35**, 354 (1986); (c) B. G. R. Rudberg and M. Johnson (unpublished).
[8] D. Rostkier-Edelstein, M. Urbakh, and A. Nitzan, J. Chem. Phys. **101**, 8224 (1994).
[9] K. L. Sebastian and G. Doyen, J. Chem. Phys. **99**, 6677 (1993).
[10] J. K. Schmickler, Surf. Sci. **335**, 416 (1995).
[11] Note that because the structures are defined on the grid, the rectangular form of the tip seen in Fig. 2(b) represents only the infinite resolution limit. Similarly, all dimensions given here are defined only within the grid resolution. Exact details concerning the dimensions in terms of grid units are provided in Sec. III.
[12] J. Hautman, J. W. Halley, and Y.-J. Rhee, J. Chem. Phys. **91**, 467 (1989).
[13] R. N. Barnett, U. Landman, and C. L. Cleveland, J. Chem. Phys. **88**, 4420 (1988).
[14] See, for example, Y. Gurevich, Y. Y. Pleksov, and Z. A. Rotenberg, *Photoelectrochemistry* (Consultant Bureau, New York, 1980); J. Bockris and S. U. M. Khan, *Surface Electrochemistry* (Plenum, New York, 1993).
[15] K. A. Motakabbir and P. J. Rossky, Chem. Phys. **129**, 253 (1989).
[16] That this may be sufficient is indicated by the fact that even though the average, over the grid, of the polarizability part (the r^{-4} terms) in the electron–water pseudopotential is only $\sim$0.15 eV, using the coefficients of these r^{-4} terms as effective polarizabilities in a calculation of the optical dielectric constant from the Clausius–Mossotti equation yields $\epsilon_\infty \sim 1.62$ which will lead to an estimated value $\sim$1 eV for the barrier lowering.
[17] H. Tal-Ezer and R. Kosslof, J. Chem. Phys. **81**, 3967 (1984).
[18] R. Kosloff, J. Phys. Chem. **92**, 2087 (1988).
[19] D. J. Tannor and D. E. Weeks, J. Chem. Phys. **98**, 3884 (1993).
[20] $g(z)$ is taken such that $|g(z)|^2$ is normalized to unity in the interval $-Lz/2 \ldots Lz/2$.
[21] T. Seidman and W. H. Miller, J. Chem. Phys. **96**, 4412 (1992); **97**, 2499 (1992).
[22] D. Neuhauser and M. Baer, J. Chem. Phys. **90**; 4351; **91**, 4651 (1989); I. Last, D. Neuhauser, and M. Baer, *ibid.* **96**, 2017 (1992).
[23] The accuracy obtained with different choices of parameters can be checked against results obtained with the analytically solvable square well or Ekhart models.
[24] W. H. Miller, S. D. Schwartz, and J. W. Tromp, J. Chem. Phys. **79**, 4889 (1983).
[25] W. H. Miller, J. Chem. Phys. **61**, 1823 (1974).
[26] R. Kosloff, Annu. Rev. Phys. Chem. **45**, 147 (1994).
[27] R. Baer and R. Kosloff (to be published).
[28] D. Neuhauser, J. Chem. Phys. **95**, 4927 (1991).